

Preparation of Nickel-Cobalt Layered Double Hydroxides for the Battery-like Electrodes in Rotor–Stator Reactor

Ya Ling Li^{1,2,3}, Lu Hai Li³, Mei Juan Cao³, Kun Dong⁴, Jie Xin Wang^{1,2}, Xiao Fei Zeng^{1,2}, Jian Feng Chen^{1,2}, Lei Shao^{1,2,*}

¹ State Key Laboratory of Organic–Inorganic Composites, Beijing University of Chemical Technology, Beijing 100029, PR China

² Research Center of the Ministry of Education for High Gravity Engineering and Technology, Beijing University of Chemical Technology, Beijing 100029, PR China

³ Beijing Engineering Research Center of Printed Electronics, Beijing Institute of Graphic Communication, Beijing 102600, PR China

⁴ Beijing Key Laboratory of Ionic Liquids Clean Process, Institute Process Engineering, Chinese Academy of Sciences, Beijing 100190, PR China

*E-mail: shaol@mail.buct.edu.cn

Received: 11 January 2017 / Accepted: 7 February 2017 / Published: 12 March 2017

Nickel-cobalt layered double hydroxides (NiCo LDHs) with different Ni/Co ratios were prepared using rotor-stator reactor technology. The morphology, crystal structure, pore size distribution and electrochemical properties were characterized and the band structure was calculated with LDA+U method in CASTEP code based on density functional theory. The results show that the band gap value of Ni₅Co₃O₁₆H₁₆ decreases compared to that of Ni₈O₁₆H₁₆. The pore size increases and the pore size distribution widens with the increasing cobalt content in the NiCo LDHs. The NiCo LDH with a Ni/Co ratio of 2:1 has a surface area of 139.9 m² g⁻¹ and a specific capacity of 176.7 mA h g⁻¹ at a current density of 1 A g⁻¹ in 6 M KOH. The electrode also exhibits good cycling stability and the capacity retention still remains 98 % after 1000 cycles.

Keywords: nickel-cobalt layered double hydroxides; rotor-stator reactor; electrochemical property; battery-type electrode; supercapacitors;

1. INTRODUCTION

Supercapacitors (SCs) have attracted much attention because they have a fast charge and discharge rate, high power density and long cycle life. Currently, carbon materials are the mostly used commercial supercapacitor electrode materials. They have good cycling stability and high maximum power density, but do not exhibit high specific capacitance or energy density due to the limitation of

reversible ion absorption at the electrode/electrolyte interface. Pseudocapacitive materials based on transitional metal oxides or conducting polymers such as RuO_2 , MnO_2 , Fe_2O_3 , poly(3,4-ethylenedioxythiophene), polyaniline, polythiophene and their composites can achieve high energy density and good rate capability. [1-6] There are usually two methods to produce electrode materials with good electrochemical performance. One is the fabrication of in-situ synthesized active materials on the surface of current collectors such as nickel foam or carbon cloth, for improving electron transport among active materials and electrical contact between the active materials and the current collectors. [7-8] The other is the preparation of nanoscale materials with large surface area and uniform pore size distribution [9-10] or doped materials [11-12] with good intrinsic conductivity. These materials can improve the electrode/electrolyte contact area and thus enhance the electrolyte ion diffusion rate or improve the cycling stability of supercapacitor electrodes.

In recent years, $\text{Ni}(\text{OH})_2$, [13-16] $\text{Co}(\text{OH})_2$, [17] nickel cobalt layered double hydroxides (NiCo LDHs) [18-20] and nickel oxides [21] have been studied extensively. The substitution of cobalt for nickel in the binary metallic hydroxides can reduce the resistance of the electrode and improve the electrochemical activities. [22] The conventional preparation methods include the electrodeposition method, [7] solvothermal method [23] and co-precipitation method. [24] In consideration of the strong mass transfer [25-26] and the facile continuous process, the rotor-stator reactor (RSR) technology has unique advantage for the large-scale synthesis of NiCo LDHs with uniform components. Moreover, it is important to note that these nickel- or cobalt- based materials should be described as battery-behavior electrode materials in fact and capacity is appropriate to represent electrocapacitive performance. [27-28]

In this work, we present a novel method to prepare NiCo LDHs in RSR. The effects of the ratio of Ni/Co on the pore size distribution of NiCo LDHs and the electrochemical properties of the corresponding battery-like electrodes were studied. The band structures of the pure $\text{Ni}(\text{OH})_2$ and NiCo LDH were calculated with the density functional theory. The as-obtained NiCo LDH with the Ni/Co ratio of 2:1 exhibits a uniform pore size distribution and superior electrochemical property.

2. EXPERIMENTAL

2.1 Synthesis of NiCo LDH nanosheets

NiCo LDHs samples were prepared in the same RSR apparatus as described in our previous paper. [29] Firstly, nickel nitrate and cobalt nitrate were dissolved into water to obtain 0.1 M mixed solution with varied Ni/Co molar ratios. Then, NaOH was dissolved into water to obtain 0.2 M NaOH solution. The above solutions with equal volumes were heated to 50 °C, respectively and then simultaneously pumped at a flow rate of 15.3 L h⁻¹ into the RSR with a rotating speed of 1000 rpm. The solutions reacted in the RSR and the product was collected and stood for some time. Then, the supernatant clear solution was removed and the solid was centrifuged and washed with distilled water and ethanol for several times. Finally, the NiCo LDHs with different Ni/Co ratios were dried in an electronic oven at 110 °C for 6 h.

2.2 Characterization and electrochemical measurement

The real Ni/Co molar ratio of the NiCo LDHs was determined by an inductive coupled plasma emission spectrometer (ICP, PerkinElmer, Optima 8300 Series). The morphology of the as-obtained NiCo LDHs was observed on a field emission scanning electron microscope (FESEM, Hitachi, SU8020). The crystal structure was measured on an X-ray diffractometer (XRD, Rigaku, Dmax/2200PC). The nitrogen adsorption/desorption isotherm at 77K was recorded on an automated surface area and pore size analyzer (Quantachrome, Quadrasorb SI). The chemical valence of Ni and Co in NiCo LDHs was analyzed by an X-ray photoelectron spectroscopy (XPS, Thermofisher, ESCALAB 250Xi) using Al K α radiation (1486.71 eV) and the spectra was corrected using C1s line at 284.8 eV.

The cyclic voltammetry (CV), galvanostatic charge/discharge (GCD), electrochemical impedance spectroscopy (EIS) measurements were conducted in 6M KOH solution with a potentiostat galvanostat (AUTOLAB PGSTAT302N). The battery-like electrode was prepared by mixing the as-obtained NiCo LDHs, acetylene black and polyvinylidene difluoride (PVDF) at a ratio of 80:10:10 in N-methylpyrrolidone (NMP) and coating the well-mixed slurry onto a nickel foam within an area of $1 \times 1 \text{ cm}^2$ and then dried at 120°C overnight in an oven. A platinum plate electrode and Hg/HgO electrode were used as counter electrode and reference electrode, respectively. The EIS measurement was performed in the frequency range from 10^{-3} Hz to 100,000 Hz at an open circuit potential.

3. RESULTS AND DISCUSSION

3.1 Morphology and crystal structure

The real Ni/Co molar ratio of NiCo LDHs determined by ICP is shown in Table 1, which are consistent with the initial ratio in original solution. The result is different from the Ni/Co molar ratio in the NiCo LDHs prepared with hydrothermal method, [30] indicating that the NiCo LDHs prepared in the RSR have uniform components due to the super micro-mixing effect of the RSR technology.

Table 1. ICP data of the NiCo LDHs

Sample No.	Initial Ni/Co molar ratio	Ni content in NiCo LDHs (mg/Kg)	Co content in NiCo LDHs (mg/Kg)	Real Ni/Co molar ratio
1	2:1	396000	201100	$\approx 2:1$
2	1:1	310300	312400	$\approx 1:1$
3	1:2	209800	421500	$\approx 1:2$

Fig.1 shows the SEM images and XRD patterns of the as-prepared NiCo LDHs. The pure Ni(OH) $_2$ is plate-like as shown in Fig.1a, and many small holes are present in the stacked nanosheets. Similar holes are observed in NiCo LDHs with the Ni/Co ratio of 2:1 and 1:1 (Fig.1b and 1c). These holes can not only improve the contact area between the electrolyte and the active electrode, but also facilitate the electrolyte ion diffusion in electrodes. The diameter of the NiCo LDH plate with the

Ni/Co ratio of 1:2 is about 100 nm (Fig.1d). As can be seen from Fig.1e plates and small particles co-exist in pure $\text{Co}(\text{OH})_2$. XRD patterns in Fig.1f reveal that the diffraction peaks match well with those of nickel hydroxide (JCPDS card No.14-0117) or cobalt hydroxide (JCPDS card No.51-1731). The rough and broad peaks observed in the XRD pattern of $\text{Co}(\text{OH})_2$ are attributed to the poor crystalline structure or small particle size.

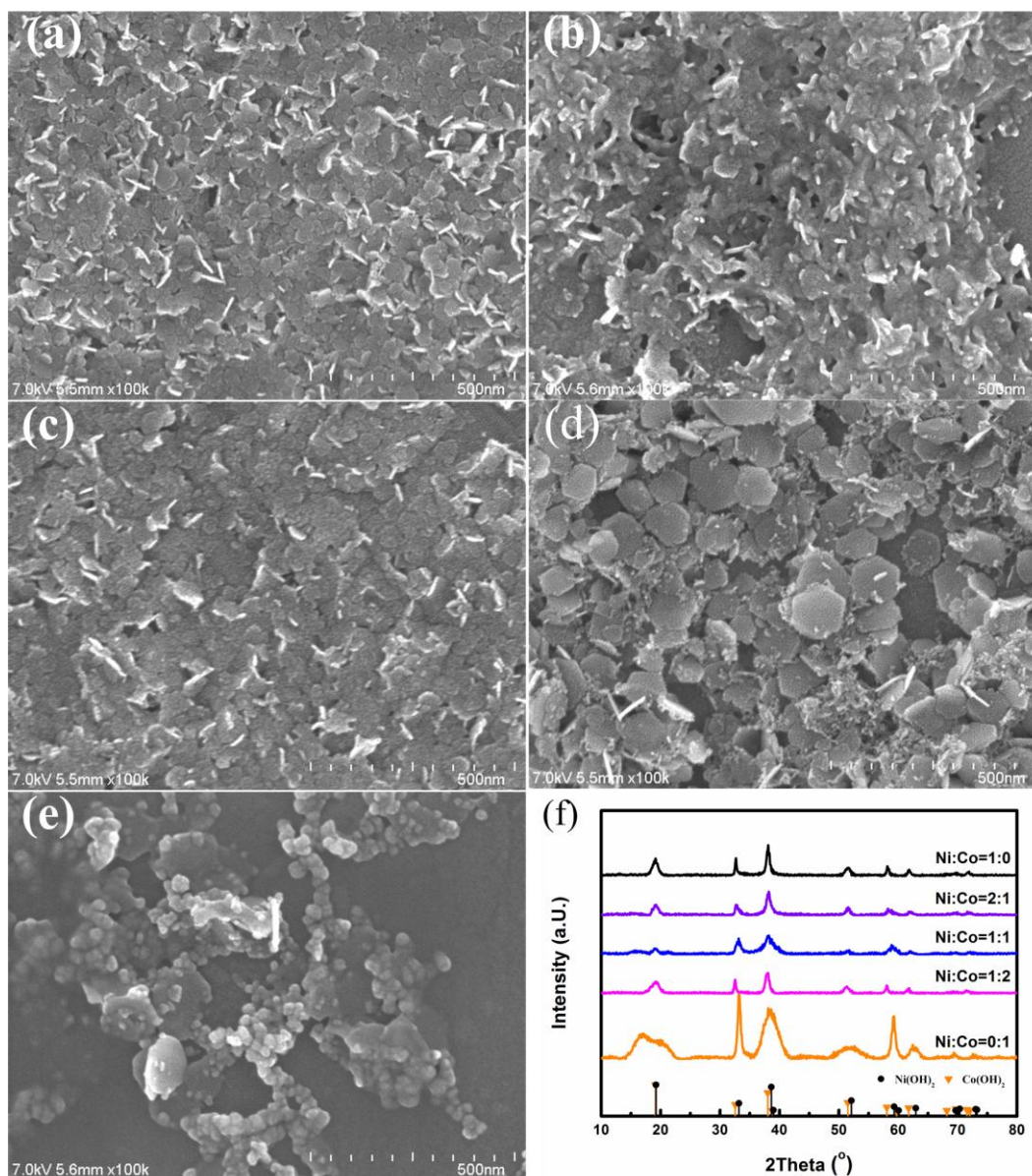


Figure 1. SEM images of NiCo LDHs with the Ni/Co ratio of 1:0 (a), 2:1 (b), 1:1 (c), 1:2 (d), 0:1 (e), and corresponding XRD patterns (f).

Specific surface area and pore size distribution have a significant effect on the electrochemical properties. N_2 adsorption/desorption isotherm measurements were performed to investigate the effect of Co content in the NiCo LDHs on the pore size distribution. The specific surface area was calculated using Brunauer-Emmett-Teller (BET) method. The pore volume and pore size distribution of the samples were obtained from the N_2 desorption branches using Barrett-Joyner-Halenda (BJH) method.

Fig.2a indicates that the Ni/Co ratio has great effect on the shape of the hysteresis loop as a result of the formation of different types of pores in the NiCo LDH nanosheets or particles. The loops of pure Ni(OH)₂ and the NiCo LDH with Ni/Co ratio of 2:1 are Type H2(a) isotherms with steep desorption branch associated with pore-blocking/percolation in a narrow range of pore necks, while the shapes of the NiCo LDHs with Ni/Co ratio of 1:1 and 1:2 are Type H2(b) loops related to pore blocking with a relatively large size distribution of neck widths. [31] The pure Co(OH)₂ gives rise to the Type H4 isotherm with aggregated crystals. The specific surface areas of the products with the Ni/Co ratio of 1:0, 2:1, 1:1, 1:2 and 0:1 are 188.5, 139.9, 95.6, 85.4 and 83.4 m² g⁻¹, respectively. The surface area decreases with the increasing cobalt content. The surface area of NiCo LDH with a Ni/Co ratio of 2:1 is larger than that of the CoNi LDH reported by Xie, et al. [32]. Fig.2b shows the pore size distribution of the as-prepared hydroxides. The mesoporous structures exist in pure Ni(OH)₂ and the NiCo LDH with Ni/Co ratio of 2:1, and the most probable pore diameters are 3.8 nm and 4.0 nm, respectively. When the Ni/Co ratio increases to 1:1, the pore size increases to about 7.9 nm and the size distribution widens, which are favourable for the electrolyte diffusion. There are relative large pores centered at 12.4 nm in the NiCo LDH with Ni/Co ratio of 1:2. The Co(OH)₂ exhibits a broad pore size distribution ranging from 5 to 70 nm.

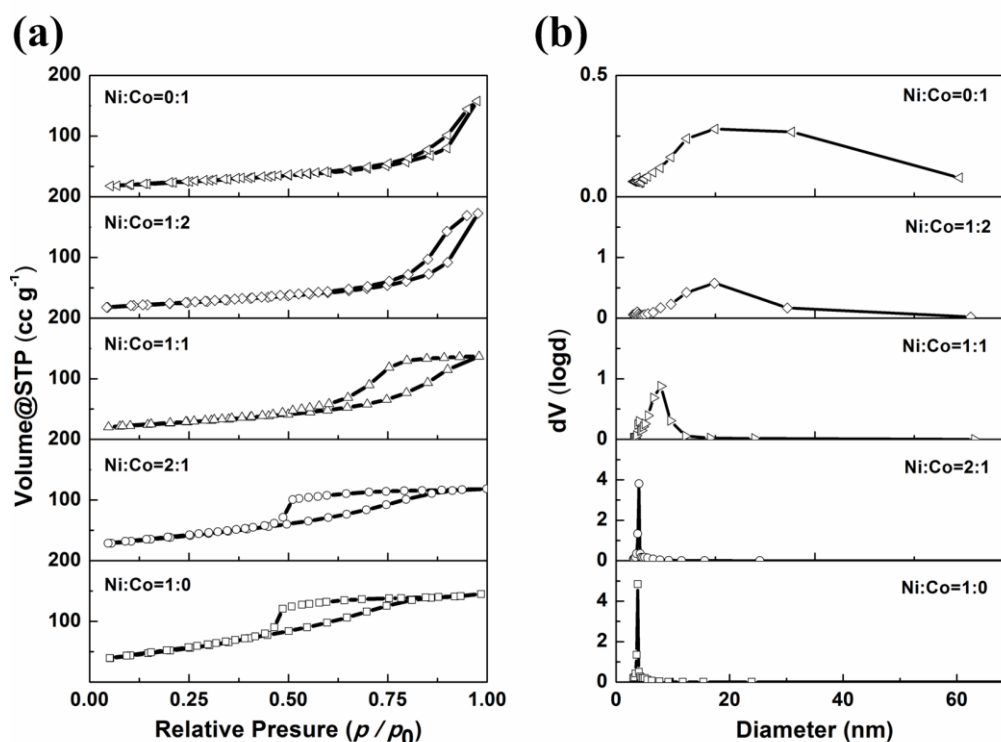


Figure 2. N₂ adsorption/desorption isotherm loop (a) and corresponding pore size distribution based on BJH method (b) of the obtained NiCo LDHs.

3.2 Electrochemical properties of the as-obtained materials

Fig.3 shows the cyclic voltammetry (CV) curves of the NiCo-LDH electrodes in 6 M KOH solution at 5 mV s⁻¹. In Fig.3a, the anodic and cathodic peaks of pure Ni(OH)₂ centered at 0.48 V and

0.29 V, respectively, which are attributed to the transformation between $\text{Ni}(\text{OH})_2$ and NiOOH . [33] The integrated area of the $\text{Co}(\text{OH})_2$ curve is almost negligible, demonstrating a low specific capacitance value of the $\text{Co}(\text{OH})_2$ electrode. The shapes of the anodic peaks in the NiCo LDHs are obviously different due to the different Ni/Co ratios. The single broad anodic peak in the NiCo LDH with Ni/Co ratio of 2:1 may be caused by the uniform doping of cobalt into nickel hydroxide crystal. The integral area of the NiCo LDH (Ni/Co = 2:1) curve is larger than the other two NiCo LDHs (Ni/Co = 1:1 and 1:2), demonstrating its good electrochemical properties.

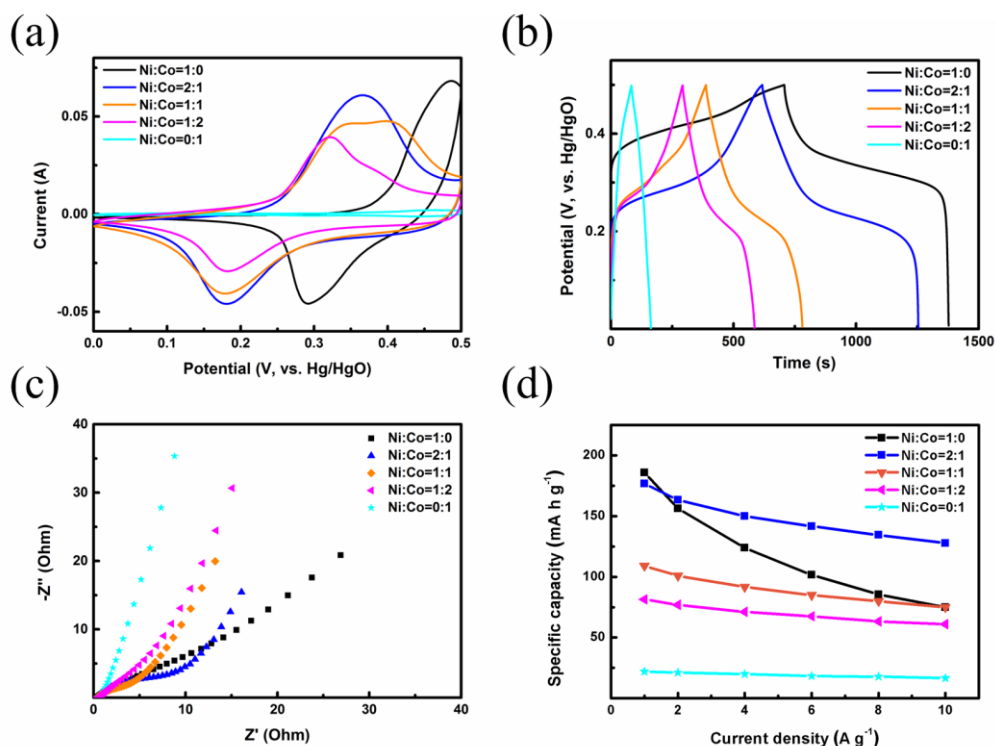


Figure 3. CV curves at a scan rate of 5 mV s^{-1} (a), GCD curves at a current density of 1 A g^{-1} (b), Nyquist plots (c) and specific capacity versus current densities (d) of the as-obtained NiCo LDHs electrodes.

The galvanostatic charge-discharge (GCD) curves at a current density of 1 A g^{-1} and Nyquist plots of the NiCo LDH electrodes are shown in Fig.3b and Fig.3c, respectively. The voltage platform observed in Fig.3b demonstrate the battery-type behaviour and so specific capacity was used to evaluate the electrochemical performance instead of specific capacitance usually used in supercapacitors.[23] The GCD tests of the NiCo LDHs at various current densities were also conducted and the calculated specific capacity versus current density is shown in Fig.3d. The slope of the EIS spectrum (Fig.3c) of the NiCo LDH electrode becomes larger in low frequency range with increasing cobalt content, demonstrating that cobalt can enhance the conductivity of the NiCo LDH electrodes. The result was also confirmed by the following calculation with the density functional theory (DFT) method. As shown in Fig. 3d, the specific capacity of the NiCo LDH electrode at a current density decreased with the increasing cobalt content. The pure $\text{Ni}(\text{OH})_2$ electrode has the largest specific capacity of 186 mA h g^{-1} at 1 A g^{-1} , whereas, it has the poorest capacity retention and the specific capacity decreases to 75 mA h g^{-1} at 10 A g^{-1} . The NiCo LDH electrode with a Ni/Co ratio

of 2:1 exhibits a relatively high specific capacity of $176.7 \text{ mA h g}^{-1}$ at 1 A g^{-1} and retains $127.8 \text{ mA h g}^{-1}$ at 10 A g^{-1} . The $\text{Ni}(\text{OH})_2$ prepared in RSR exhibits better electrochemical properties than the previous work. [34] Although the capacity of the NiCo LDH prepared in RSR is not higher than the reported work [23], it may be due to the different active material loading mass in the active electrode and the difference between the coating electrode and the active material electrode directly grown on the current collector. The RSR technology can be easily used in the industrialized production and obtain NiCo LDHs with large surface area and provides us a new technology.

3.3 DFT calculations of $\text{Ni}(\text{OH})_2$ and NiCo LDH

The DFT method was used to calculate the band gap of the pure $\text{Ni}(\text{OH})_2$ and NiCo LDH (Ni/Co \approx 2:1) in Materials Studio CASTEP. The original unit cell of $\text{Ni}(\text{OH})_2$ was proposed from the ICSD database (No.28101) and the super cell of $\text{Ni}_8\text{O}_{16}\text{H}_{16}$ was constructed as shown in Fig.4a. The geometry structure was optimized at first and then the energy was calculated using the generalized gradient approach (GGA) and Perdew-Burke-Ernzerhof (PBE) with LDA+U method. The energy cutoff and SCF tolerance were 340 eV and 2×10^{-6} eV/atom respectively, and the Monkhorst-Pack grid was set as $4 \times 4 \times 4$ for geometry optimization and $6 \times 6 \times 4$ for energy calculation. The LDA+U calculations of $\text{Ni}_8\text{O}_{16}\text{H}_{16}$ using different Hubbard U values such as 2.5 eV, 4.0 eV and 5.5 eV for the Ni-3d orbital were performed and are shown in Fig.4b, Fig.4c and Fig.4d, and the calculated band gap values are 1.612 eV, 2.129 eV and 2.453 eV, respectively. The band gap of $\text{Ni}(\text{OH})_2$ calculated using the U value of 4.0 eV is in good agreement with previous results. [35-37] Therefore, the band structure of $\text{Ni}_5\text{Co}_3\text{O}_{16}\text{H}_{16}$ was also calculated using the U value of 4.0 eV for both Ni-3d and Co-3d orbitals.

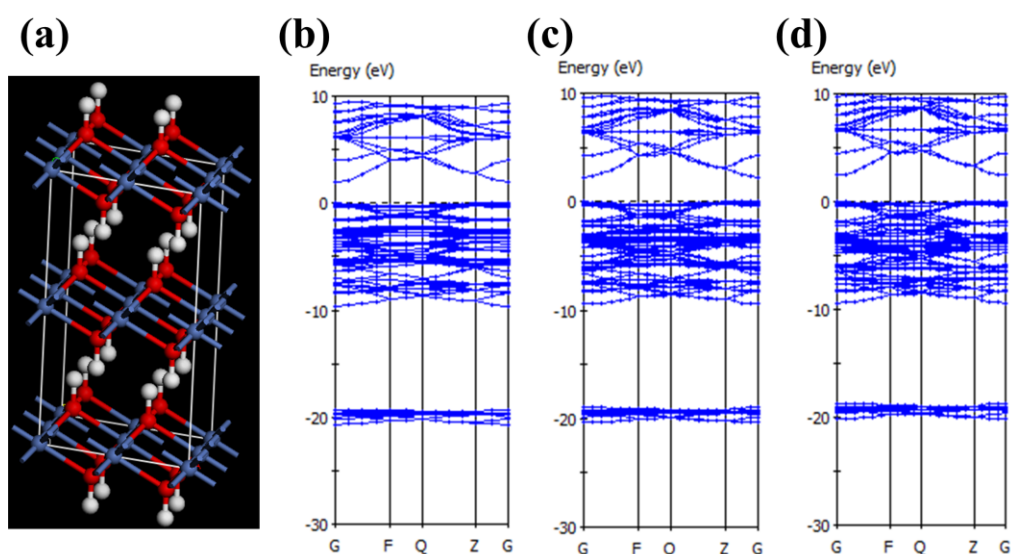


Figure 4. Super cell of $\text{Ni}_8\text{O}_{16}\text{H}_{16}$ (where Ni element is shown in blue, O element is in red and H element is in white) (a) and the band structures of $\text{Ni}_8\text{O}_{16}\text{H}_{16}$ with $U=2.5 \text{ eV}$ (b), $U=4.0 \text{ eV}$ (c) and $U=5.5 \text{ eV}$ (d).

The symmetry systems of $\text{Ni}_5\text{Co}_3\text{O}_{16}\text{H}_{16}$ were constructed with Co substituted for Ni atoms in different sites of $\text{Ni}_8\text{O}_{16}\text{H}_{16}$ as shown in Fig.5a-5d. The geometry and energy were also calculated using the same parameters. Based on the band structures as shown in Fig.5e-5h, the band gap values are 1.003 eV, 1.037 eV, 1.018 eV and 0.553 eV, respectively. The NiCo LDH with narrow band gap demonstrates that cobalt substituting for nickel in the nickel hydroxide crystal lattice could enhance the electronic conduction.

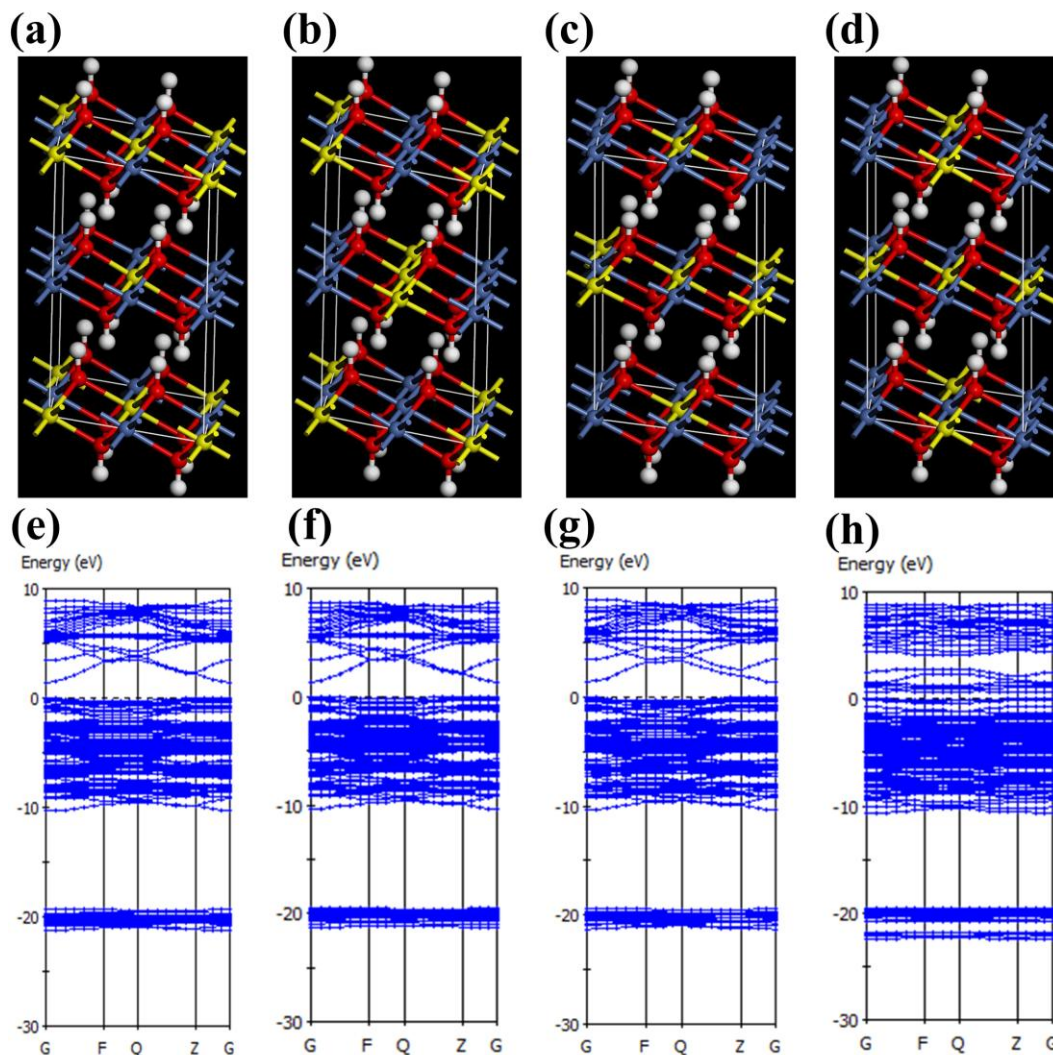


Figure 5. Super cells of $\text{Ni}_5\text{Co}_3\text{O}_{16}\text{H}_{16}$ (where Ni element is shown in blue, O element is in red, H element is in white and Co element is marked in yellow) with different Co-substitution sites (a, b, c, d) and the corresponding band structures of $\text{Ni}_5\text{Co}_3\text{O}_{16}\text{H}_{16}$ with the U value of 4.0 eV (e, f, g, h).

3.4 XPS and electrochemical properties of the NiCo LDH (Ni/Co = 2:1)

The chemical and electronic states of the NiCo LDH with a Ni/Co ratio of 2:1 were further studied by X-ray photoelectron spectroscopy (XPS). There are two shakeup satellites (indicated as

“Sat”) and two spin-orbit peaks at 856.0 eV and 873.7 eV related to Ni 2p_{3/2} and Ni 2p_{1/2} in Fig.6a, respectively. As for the Co 2p spectrum (Fig.6b), there are two peaks located at 781.1 eV and 796.9 eV, which are contributed to Co 2p_{3/2} and Co 2p_{1/2}, respectively. These results are in good agreement with the reported values. [38-39]

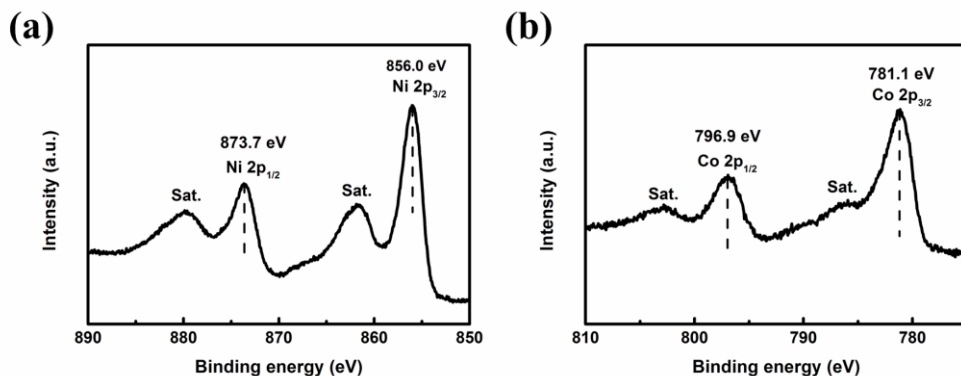


Figure 6. XPS spectra of Ni 2p (a) and Co 2p (b) of NiCo LDH (Ni/Co=2:1).

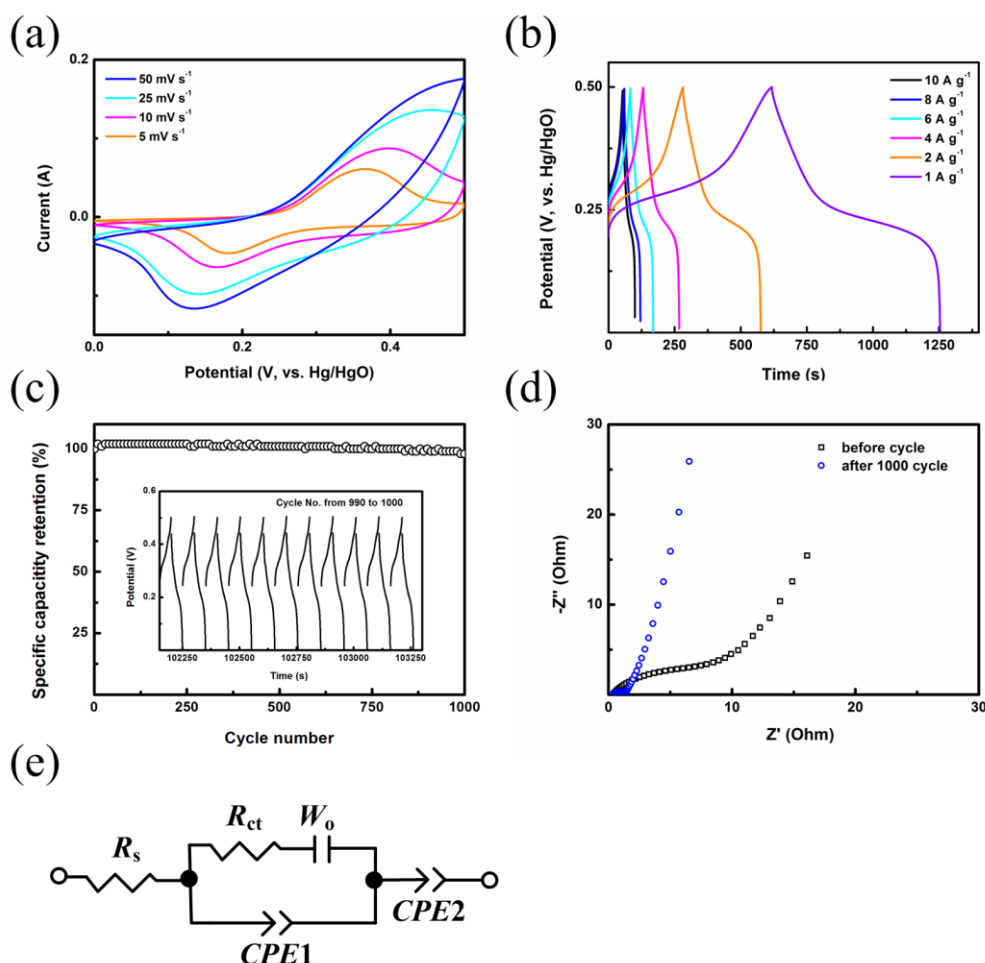


Figure 7. CV curves at different scan rates (a), GCD curves at different current densities (b), specific capacity versus current densities (c), Cycling behavior measured at a current density of 10 A g⁻¹ (inset shows GCD curves of the NiCo LDH electrode between 990 and 1000 cycles) of the NiCo LDH (Ni/Co=2:1) electrode (d), Nyquist plots of the NiCo LDH (Ni/Co=2:1) electrode before and after 1000 cycles (e) and the fitting equivalent circuit (f).

The electrochemical properties of the NiCo LDH with a Ni/Co ratio of 2:1 electrode are shown in Fig. 7. The CV curves at different scan rate are shown in Fig.7a and the peak spacing between the anodic and cathode peaks increased with the increasing scan rate because the OH⁻ ions only utilized the outer surface of the NiCo LDH electrode at a high scan rate. Fig.7b shows the charge/discharge curves at various current densities of 10, 8, 6, 4, 2 and 1 A g⁻¹ between 0 and 0.5 V and the calculated specific capacity has been shown in Fig.3d.

The charged and discharged curves show good symmetry indicating that the NiCo LDH electrode has good electrochemical reversibility. The cycling stability of the NiCo LDH (Ni/Co=2:1) electrode charged and discharged at 10 A g⁻¹ was also studied and the GCD curves between 990 and 1000 cycles are shown in Fig.7c. The specific capacity after 1000 cycles is 98 % of the initial specific capacity. The EIS spectra in Fig.7d was fitted well using the equivalent circuit as shown in Fig.7e, and in the circuit, W_0 and CPE demonstrate Warburg impedance and constant phase element. The combined resistance (R_s) and the interfacial charge transfer resistance (R_{ct}) values were 0.4 Ω and 6.38 Ω in the NiCo LDH with a Ni/Co ratio of 2:1, respectively. R_s value remained 0.4 Ω while R_{ct} value decreased to 0.94 Ω after the electrode was charged and discharged for 1000 cycles, which denotes that the electrode was activated by the continuous charged/discharged cycles.

4. CONCLUSIONS

In summary, the NiCo LDHs with different Ni/Co ratios were prepared in the RSR and the pore size distribution becomes wider with the increasing cobalt content in the NiCo LDHs. The band structure of Ni(OH)₂ and NiCo LDH were calculated using LDA+U method with DFT theory. The band gap value of NiCo LDH is smaller than that of pure Ni(OH)₂. Cobalt substitution for nickel can improve the rate capacity of the nickel-based hydroxide electrodes. The NiCo LDH electrode with a Ni/Co ratio of 2:1 achieved a high surface area and good electrochemical properties.

ACKNOWLEDGEMENTS

This work was supported by the National Key Research Program of China (2016YFA0201701/2016YFA0201700), National Natural Science Foundation of China (21622601/21646013), Beijing Municipal Science and Technology Project (Z151100003315005), Collaborative Innovation Center of Green Printing & Publishing Technology (CGPT), Research on Common Key Technology of Thin Film Printed Electronics, Beijing Municipal Commission Education (SQKM201710015009), and Project of BIGC (20190116002/039, Eb201602). We thank Prof. Xipeng Liu for providing ICSD data.

References

1. S. Cho, M. Kim and J. Jang, *ACS Appl. Mater. Inter.*, 7 (2015) 10213.
2. S. B. Yoon and K. B. Kim, *Electrochim. Acta*, 106 (2013) 135.
3. I. Shown, A. Ganguly, L. C. Chen and K. H. Chen, *Energy Sci. Eng.*, 3 (2015) 2.
4. C. Wan, M. Cheng, Q. Zhang and N. Jia, *Powder Technol.*, 235 (2013) 706.
5. Q. Lu and Y. Zhou, *J. Power Sources*, 196 (2011) 4088.

6. X. Tang, R. Jia, T. Zhai and H. Xia, *ACS Appl. Mater. Inter.*, 7 (2015) 27518.
7. J. Xing, S. Wu and K. Y. S. Ng, *RSC Adv.*, 5 (2015) 88780.
8. A. D. Jagadale, G. Guan, X. Du, X. Hao, X. Li and A. Abudula, *RSC Adv.*, 5 (2015) 56942.
9. C. L. Wang, H. L. Qu, T. Peng, K. Y. Mei, Y. Qiu, Y. Lu, Y. S. Luo and B. H. Yu, *Electrochim. Acta*, 191 (2016) 133.
10. Y. Kim, E. S. Cho, S. J. Park and S. Kim, *J. Ind. Eng. Chem.*, 33 (2016) 108.
11. W. Ma, L. Wang, J. Xue and H. Cui, *J. Alloy. Compd.*, 662 (2016) 315.
12. A. M. Hashem, H. M. Abuzeid, N. Narayanan, H. Ehrenberg and C. M. Julien, *Mater. Chem. Phys.*, 130 (2011) 33.
13. W. Jiao and L. Zhang, *Curr. Appl. Phys.*, 16 (2016) 115.
14. Z. J. Li, W. Y. Zhang, Y. L. Su, H. Y. Wang and B. C. Yang, *Appl. Surf. Sci.*, 383 (2016) 268.
15. J. S. Chen, Y. Gui and D. J. Blackwood, *Electrochim. Acta*, 188 (2016) 863.
16. H. Cui, J. Xue and M. Wang, *Adv. Powder Technol.*, 26 (2015) 434.
17. C. Mondal, M. Ganguly, P.K. Manna, S.M. Yusuf and T. Pal, *Langmuir*, 29 (2013) 9179.
18. D. Yang, *J. Power Sources*, 198 (2012) 416.
19. T. Li, G. H. Li, L. H. Li, L. Liu, Y. Xu, H. Y. Ding and T. Zhang, *ACS Appl. Mater. Inter.*, 8 (2016) 2562.
20. Y. Cheng, H. Zhang, C.V. Varanasi and J. Liu, *Energ. Environ. Sci.*, 6 (2013) 3314.
21. M. M. Sk, C. Y. Yue, K. Ghosh and R. K. Jena, *J. Power Sources*, 308 (2016) 121.
22. H. N. Ma, J. He, D. B. Xiong, J. S. Wu, Q. Q. Li, V. Dravid and Y. F. Zhao, *ACS Appl. Mater. Inter.*, 8 (2016) 1992.
23. W. Quan, Z. Tang, Y. Hong, S. Wang and Z. Zhang, *Electrochim. Acta*, 182 (2015) 445.
24. C. H. Wang, X. Zhang, X. Z. Sun and Y. W. Ma, *Electrochim. Acta*, 191 (2016) 329.
25. G. W. Chu, Y. H. Song, H. J. Yang, J. M. Chen, H. Chen and J. F. Chen, *Chem. Eng. J.*, 128 (2007) 191.
26. Y. W. Li, S. W. Wang, B. C. Sun, M. Arowo, H. K. Zou, J. F. Chen and L. Shao, *Chem. Eng. Sci.*, 134 (2015) 521.
27. C. F. Yu and L. Y. Lin, *J. Colloid Interf. Sci.*, 482 (2016) 1.
28. T. Brousse, D. Bélanger and J. W. Long, *J. Electrochem. Soc.*, 162 (2015) A5185.
29. Y. L. Li, L. H. Li, G. W. Chu, X. F. Xiao, J. F. Chen and L. Shao, *Int. J. Electrochem. Sci.*, 11 (2016) 9644.
30. J. Jiang, A. Zhang, L. Li and L. Ai, *J. Power Sources*, 278 (2015) 445.
31. M. Thommes, K. Kaneko, A. V. Neimark, J. P. Olivier, F. Rodriguez-Reinoso, J. Rouquerol and K. S. W. Sing, *Pure Appl. Chem.*, 87 (2015) 1051.
32. L. J. Xie, G. H. Sun, L. F. Xie, F. Y. Su, X. M. Li, Z. Liu, Q.Q. Kong, C.X. Lu, K. X. Li and C. M. Chen, *New Carbon Mater.*, 37 (2016) 31.
33. S. Vijayakumar and G. Muralidharan, *J. Electroanal. Chem.*, 727 (2014) 53.
34. X. B. Zhou, D. X. Cao, J. C. Huang, K. Ye, S. N. Yang, T. Liu, X. W. Liu, J. L. Yin and G. L. Wang, *J. Electroanal. Chem.*, 115 (2014) 720.
35. M. Cococcioni and S. de Gironcoli, *Phys. Rev. B*, 71 (2005) 035105.
36. Z. K. Tang, W. W. Liu, D. Y. Zhang, W. M. Lau and L. M. Liu, *RSC Adv.*, 5 (2015) 77154.
37. Y.T. Zhao, Photocurrent response analysis of passive films with duplex structures [M], *North China Electric Power University* (2014).
38. L. Zhang, Q. Ding, Y. Huang, H. Gu, Y. E. Miao and T. Liu, *ACS Appl. Mater. Inter.*, 7 (2015) 22669.
39. Z. Wang, Y. Liu, C. Gao, H. Jiang and J. Zhang, *J. Mater. Chem. A*, 3 (2015) 20658.